Design, Control and Performance of Tracking Power Supply for a Linear Power Amplifier

G. Gong, S. Round and J. W. Kolar
Swiss Federal Institute of Technology (ETH) Zurich
Power Electronic Systems Laboratory
CH-8092 Zurich, SWITZERLAND
Email: gong@lem.ee.ethz.ch

Abstract - Power amplifiers are widely used in consumer and industrial applications and are based on either a linear power amplifier or switch-mode power amplifier design. By combining the linear power amplifier with a switch-mode tracking power supply, a hybrid power amplifier is formed that maintains a high quality output while having a high efficiency. This paper presents a hybrid amplifier that is constructed with a novel boost-type tracking power supply and provides an excellent performance. A design method for the output filter using the Power Supply Ratio Rejection (PSRR) of the linear power amplifier is proposed. This method ensures that the amplifier output voltage has minimal switching frequency components as well as being able to quickly track changes in the output voltage. A control system design method is presented that ensures good performance in the control of the constant inductor current of the switch-mode tracking stage and a high rejection of output voltage disturbances. A laboratory prototype experimentally verifies the theoretical analysis.

I INTRODUCTION

Power amplifiers are widely used in consumer and industrial applications such as audio systems and controllable test-equipment power sources. Presently these amplifiers are based on either a linear power amplifier or switch-mode power amplifier design. Typically the linear power amplifier produces a high quality output voltage but it also has high power losses. On the other hand the switch-mode power amplifiers have higher efficiencies but they have increased output distortion caused by the switching nature of the amplifier. By combining the linear power amplifier and a switch-mode tracking power supply, a hybrid power amplifier is produced that maintains a high quality output while having a high efficiency.

The low efficiency of linear power amplifiers is caused mainly by the voltage drop across the output power transistors since they are operating in their linear region. The amount of voltage drop and therefore the power loss is dependent on the value of the supply voltage and the output voltage level. By replacing the constant supply voltage with an adjustable voltage the power loss of the linear amplifier is reduced. A switch-mode tracking power supply can efficiently provide the linear amplifier's supply voltage, which is set at a value slightly higher than the instantaneous output voltage. The switch-mode tracking power supply can also quickly control this supply voltage to track the required changing output voltage of the power amplifier. Therefore, the voltage drop across the linear amplifier power transistors is reduced considerably and this results in a corresponding reduction of the amplifier power losses [1-3].

In the literature, majority of the switch-mode voltage tracking power supplies are based on the buck-type converter. A novel boost-type tracking power supply for linear power amplifiers, as shown in **Fig. 1(a)**, has been proposed by the authors [4]. The ideal waveforms of the tracking power supply voltages are shown in Fig. 1(b). As can be seen the positive and negative supply voltages are adjusted so they remain just above/below the required output voltage level.

The power supply stage of this hybrid power amplifier comprises of: (i) a buck stage, which uses fixed-frequency PWM current control to regulate the inductor current i_L, and could be replaced by other buck derived converters, e.g. a three-level isolated dc-dc converter, (ii) a boost stage where tolerance band control is performed to achieve an excellent dynamic behavior of the voltage level, and (iii) an output filter that reduces the supply voltage switching ripple to guarantee a good output voltage THD plus noise (THD+N) figure.

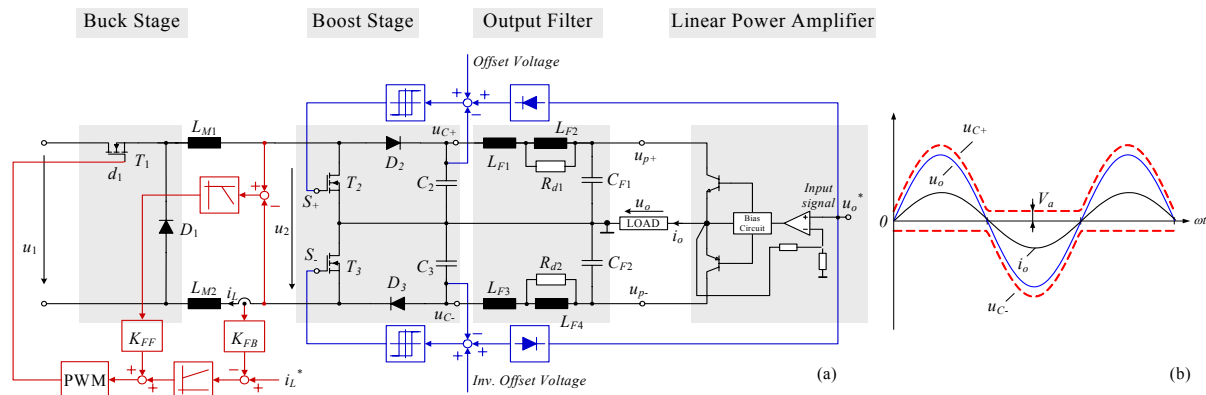This paper focuses on the main issues in designing the proposed

Fig. 1 Hybrid Power Amplifier (a) Boost-type tracking power supply providing the supply voltage for a linear power amplifier, (b) ideal power supply voltages and output voltage waveforms. Component parameters are given in the Appendix.

boost-type tracking power supply for a linear power amplifier. The basic operating principles of the proposed system are analyzed, and the dimensioning of components is given in **Section II**. The design procedure for the output filter, to minimize the switching noise influence on the output voltage, is presented in **Section III.** A small signal model of the proposed power supply is derived and the controller design using the constant current mode is presented in **Section IV**. Finally in **Section V**, an active damping scheme for the output filter is presented. Throughout the paper experimental results verify the theoretical performance of the proposed hybrid power amplifier.

II   TRACKING POWER SUPPLY DESIGN AND DIMENSIONING

A   Basic Operating Principle

The literature has proposed several different control schemes for the proposed hybrid amplifier shown in Fig. 1 [4, 5]. The simplest control scheme, which provides greatest output voltage dynamics, is to control the buck stage to ensure that there is a constant current I_L flowing in the inductors L_{M1} and L_{M2}, and then to use a hysteresis control with the boost stage transistors to regulate the output voltage. This simplified scheme of constant current control is shown in **Fig. 2**, where the input stage is now considered as a constant current source and the output filter is neglected.

Representative waveforms for the supply voltages u_{C+}, u_{C-} and output voltage u_o of the linear power amplifier are shown in **Fig. 3**. If it is assumed that the positive supply voltage, u_{C+}, is being regulated to follow the output voltage and transistor T_3 is remaining on-state in case u_{C-} is lower than the reference value then the basic principle of operation is as follows: Transistor T_2 is on since the voltage on C_2 is higher than the required voltage. As the linear power amplifier is drawing current the voltage u_{C+} will reduce until it reaches the threshold value, and at this point T_2 is turned off. The current I_L commutates into D_2 and recharges the output capacitor C_2. When the voltage u_{C+} reaches the upper bound of the tolerance band, T_2 is turned on, and the inductor current I_L now circulates through T_2 and T_3.

B   Dimension of Output Capacitors C_2 and C_3

The value of the output capacitors, C_2 and C_3, has a significant influence on the current source value and the switching frequency of the boost stage. A practical selection of the output capacitor value is to use a maximum capacitor current value that is 20% of the peak current
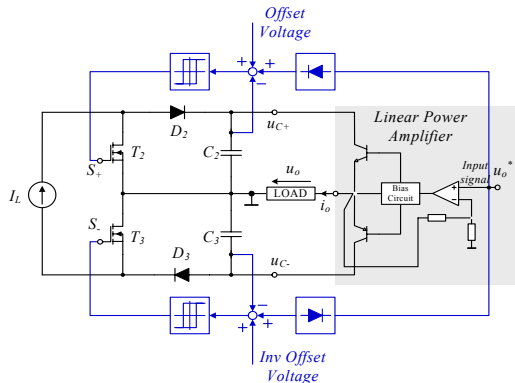
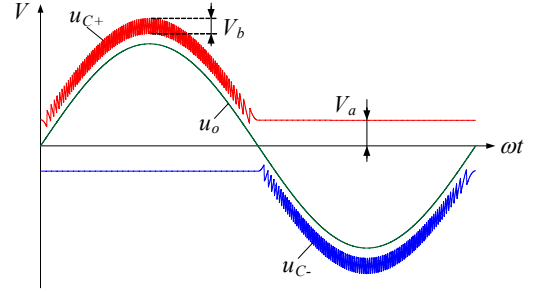**Fig. 2** Simplified scheme of the tracking power supply employing constant current control.

Fig. 3 Representative waveforms of the supply voltages u_{C+}, u_{C-} and output voltage u_o of the linear power amplifier.

of the linear power amplifier. The capacitor value then can be calculated as

$$C \approx \frac{0.2 \cdot I_{op}}{2\pi \cdot f_o \cdot V_{op}} \quad (1)$$

where I_{op} and V_{op} are the output peak current and voltage of the linear power amplifier; and f_o is the output frequency.

C   Constant Inductor Current Setting I_L

In order to ensure the required output performance, the constant inductor current I_L should always be higher than the summed current I_{sum} needed by the linear power amplifier and output capacitors, which is

$$I_{sum} = I_{op}\sin(2\pi \cdot f_o \cdot t) + 2\pi \cdot f_o \cdot C \cdot V_{op}\cos(2\pi \cdot f_o \cdot t). \quad (2)$$

Considering the inductor current ripple in the real switching system, the value of the constant inductor current I_L is selected using

$$I_L = 1.2 \cdot \max(I_{sum}) = 1.2 \cdot \sqrt{I_{op}{}^2 + (2\pi \cdot f_o \cdot C \cdot V_{op})^2}. \quad (3)$$

D   Switching Frequency Analysis

The switching frequency range of the boost switches is now analyzed and this information is used when calculating the switching losses and designing the output filter. Since the switching frequency is much higher than the output current frequency, it is assumed the charge flow of the output capacitors is balanced over a switching period. Therefore the local switching frequency f_s can be derived as

$$f_s = \frac{\frac{\alpha^2}{4} - (\sin\omega t - \frac{\alpha}{2})^2}{\alpha \cdot C \cdot V_b} \cdot I_{op}. \quad (4)$$

where V_b denotes the tolerance band voltage and α denotes the current ratio $\alpha = I_L / I_{op}$.

The maximum switching frequency therefore can be derived as

$$f_{s\_\max} = \frac{\alpha \cdot I_{op}}{4C \cdot V_b} = \frac{I_L}{4C \cdot V_b}. \quad (5)$$

and the average switching frequency can be derived as

$$f_{s\_avg} = \frac{1}{2\pi}\int_\theta^{\pi-\theta} f_s d\omega t \approx \frac{1}{2\pi}\int_0^\pi f_s d\omega t = \frac{I_{op}}{2\alpha \cdot C \cdot V_b}(\frac{2\alpha}{\pi} - \frac{1}{2}) \quad (6)$$

where the phase $\theta = \pi - \arctan^{-1}(-1/(2\pi \cdot f_o \cdot C \cdot R_L))$.
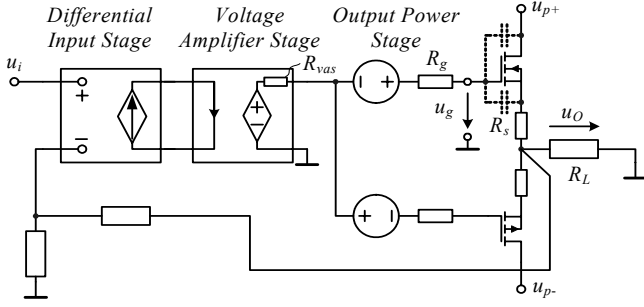
Fig. 4 Simplified equivalent circuit of a typical Class AB power amplifier.

III   OUTPUT FILTER DESIGN

As shown in **Fig. 3**, the power supply voltages for the linear power amplifier include switching frequency ripple and this can reduce the quality of the output voltage. Therefore, a filter is placed between the converter and linear power amplifier to limit the switching noise. However, the cutoff frequency of this filter should not be made too low as it can reduce the performance of the output voltage tracking.

A   PSRR Consideration of a Linear Power Amplifier

Based on this aim, the PSRR of a simplified linear power amplifier is analyzed to specify the ripple limitation of the power supply voltage. The PSRR is very dependent on the configuration and on component parameters of the linear power amplifier [6-7].

A simplified equivalent circuit of a typical Class AB linear power amplifier is shown in **Fig. 4**. The differential input stage is replaced by a voltage controlled current source, the voltage amplifier stage is substituted by a current controlled voltage source, and the output power stage is a voltage follower where MOSFETs are utilized for output stage devices instead of bipolar transistors in order to reduce the required power for the driver stage.

In order to deduce the PSRR transfer function, a block diagram of the simplified linear power amplifier is shown in **Fig. 5**. In this block diagram, $G_{po}(s)$ is the transfer function from power supply voltage u_{p+} to output voltage u_o, $G_{io}(s)$ represents the transfer function from input reference voltage u_i to output voltage u_o and K_F is the feedback gain of the linear power amplifier. Therefore, the PSRR can be obtained as
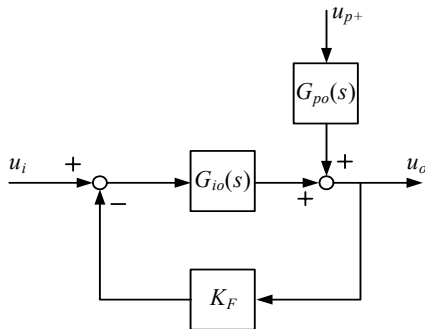

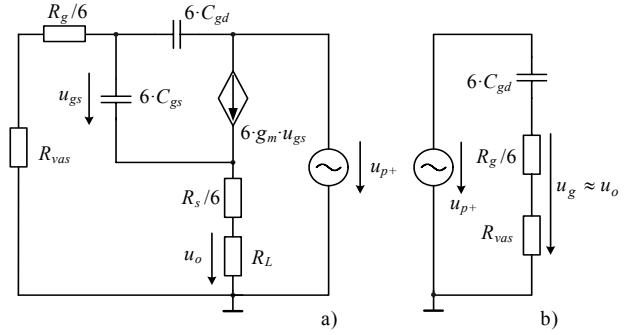**Fig. 5** Block diagram of the simplified linear power amplifier

Fig. 6 Simplified small signal model of the output stage (a) and the approximate small signal model (b) for deriving $G_{po}(s)$.

$$G_{PSRR}(s) = \frac{G_{po}(s)}{1 + G_{io}(s) \cdot K_F} . \qquad (7)$$

In experimental system, only the output power stage is supplied by the tracking power supply while the voltage gain stages are supplied by an additional "clean" power supply. Therefore, only the output stage of the linear power amplifier is considered in deriving $G_{po}(s)$. **Fig. 6** shows the simplified equivalent small signal model of the output stage (experimentally the output stage is the parallel connection of six BUZ 50B MOSFETs with individual gate resistors and source resistors) of the linear power amplifier system. This equivalent model only considers the upper leg of the output power stage. In the model the gate-to-source capacitance is defined as C_{gs}; C_{gd} is the gate-to-drain capacitance; R_g is the gate resistance; R_{vas} is the output impedance of the voltage amplifier stage; g_m is the transconductance of the MOSFET and R_L is the load resistance. Fig. 6(a) shows the simplified PSRR small signal model of the output power stage, and Fig. 6(b) illustrates the approximate model where it is assumed that the output power stage acts as an ideal voltage follower so that the output voltage u_o can be regarded being identical to the gate voltage u_g. Therefore, the transfer function $G_{po}(s)$ can be easily derived from the model in Fig. 6(b) as

$$G_{po}(s) = \frac{s C'_{gd} R_t}{s C'_{gd} R_t + 1} \qquad (8)$$

where $C_{gd}' = 6 \cdot C_{gd}$, $R_t = R_g/6 + R_{vas}$.

The magnitude curves of the calculated transfer function $G_{po}(s)$ are shown in **Fig. 7**, where the parameters obtained from the BUZ 50B datasheet and hardware are: C_{gs} = 2nF, C_{gd} = 55pF, g_m = 1.5S, R_g = 470Ω, R_{vas} = 200Ω, R_L = 20Ω. The transfer function $G_{po}(s)$ is identical to the PSRR since the voltage feedback loop of the realized experimental system uses the output of the voltage amplifier stage instead of the output voltage. The calculated PSRR from the approximate model (Fig. 6(b)) closely matches the calculated PSRR resulting from the model given in Fig. 6(a). The dominant parameters of the output stage for determining the PSRR are the gate-to-drain capacitance C_{gd}, the gate resistance R_g, and the output impedance of the voltage amplifier stage R_{vas}. In Fig. 7, it is shown that the PSRR has a slope of -20dB/decade for low frequencies, and if the frequency increases beyond the corner frequency $1/(2\pi C_{gd}'R_t)$ the linear power amplifier can no longer attenuate the supply voltage ripple and the ripple appears directly on the output voltage of the linear power amplifier. The PSRR measured in the hardware is -21dB@100kHz and
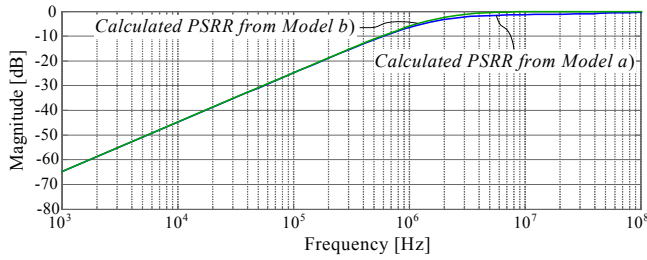
Fig. 7 Bode plots of the calculated PSRR from equivalent small signal model in Fig. 6 (a) and the approximate small signal model in Fig. 6 (b).

-14dB@200kHz, which sufficiently close to the calculated results of -24dB@100kHz and -18dB@200kHz. If closed loop control of linear power amplifier output voltage is implemented then an increased low frequency PSRR can be achieved, but this is limited by the bandwidth of the linear power amplifier.

B Output Filter Design

For linear power amplifiers, the typical THD+N figure that denotes the output voltage quality is dependent on the application, and in this paper a value of 0.1% is assumed to be suitable. The aim of the filter design is to limit the output voltage noise caused by the switching frequency ripple so as not to significantly influence the THD+N figure.

The simulated spectrum of the switching frequency voltage ripple in the output voltage of the converter without a filter is shown in **Fig. 8**. The spectrum illustrates that the switching noise is mainly between
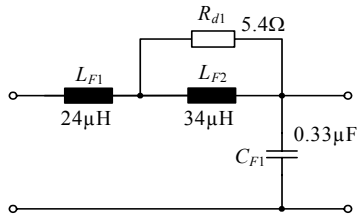

Fig. 9 Output filter topology and parameters.
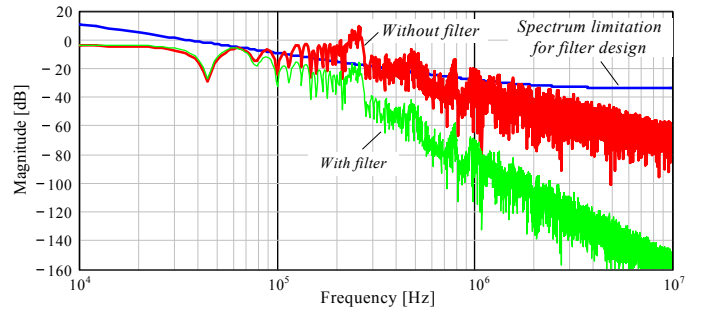

Fig. 8 Simulated tracking supply output voltage spectrum with/without filter. Simulation parameters are: I_L=15A, V_b=30 V, V_{op}=200 V, f_o=1kHz, R_L=20Ω

100kHz and 300kHz.

Before undertaking the filter design a guideline for the peak-to-peak amplitude of any output voltage frequency caused by the switching power supply must be specified, and in this case a value of less than 10% of the THD+N figure is used. The guideline is given by (9) and is shown in Fig. 8.

$$V_{guide}(s) = 0.1 \times 0.1\% \times V_{op} \cdot \frac{1}{G_{PSRR}(s)} \tag{9}$$

A filter topology is selected and the parameters of the components are calculated to fulfill the criteria, as shown in **Fig. 9**. The design of the filter parameters uses the procedure referred to in [8] and [9]. The spectrum of the filtered output voltage of the tracking power supply is shown in Fig. 8, where all the frequency components are lower than the required level. The total noise in the output voltage caused by the switching noise without the filter is about 0.6% and with the output filter the total noise figure is significantly reduced to 0.05%.

IV CONVERTER CONTROLLER DESIGN

The proposed tracking power supply is actually a buck-boost type converter. In this section, the small signal model of the converter is first derived, then feed forward control is implemented to improve the stability of the system, and finally the design for the constant current
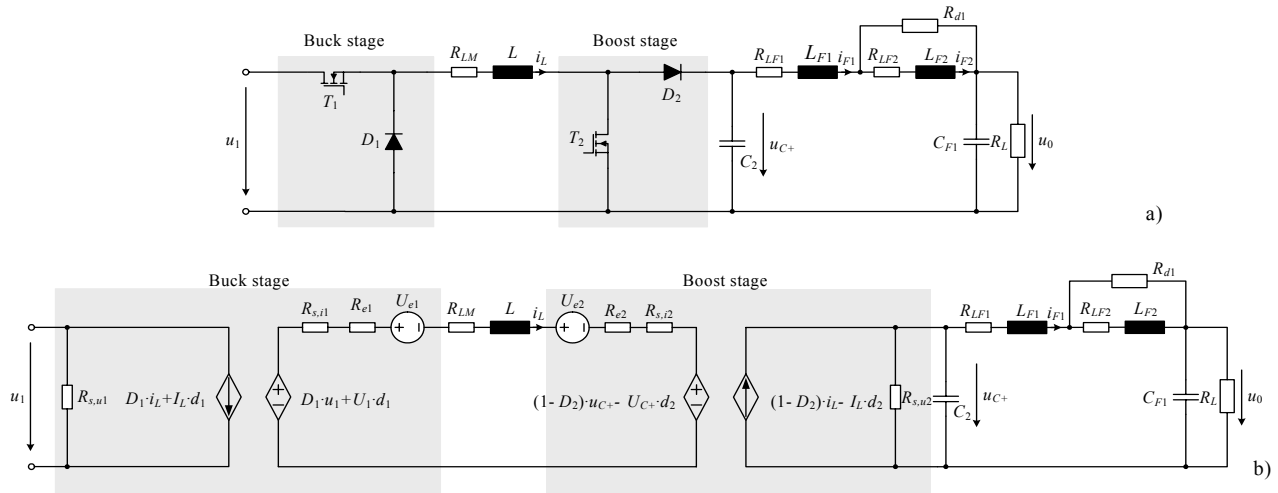

Fig. 10 Equivalent circuit of the tracking power supply when the upper output stage is operating (a), and the corresponding linearized small signal model including the main damping resistances (b).

controller is developed.

A   Linearized Small Signal Model

The equivalent circuit of the tracking power supply when the upper output stage is operating is given in **Fig. 10**(a), and the corresponding linearized small signal model including the main damping resistance is shown in Fig. 10(b). The damping resistances include the equivalent resistances R_{e1} and R_{e2} of the semiconductors in the buck stage and boost stage, the resistances $R_{s,u1}$, $R_{s,i1}$ and $R_{s,u2}$, $R_{s,i2}$ represent the switching losses of the buck stage and boost stage [10]; the resistances R_{LM}, R_{LF1} and R_{LF2} are the equivalent series resistances of the corresponding inductors. The equivalent semiconductor resistances R_{e1} and R_{e2} can be determined from

$$R_{e1} = D_1 \cdot R_{T1} + (1-D_1) \cdot R_{D1}$$
$$R_{e2} = D_2 \cdot R_{T2} + (1-D_2) \cdot R_{D2} \tag{10}$$

where D_1 and D_2 are the static duty cycle of the buck stage and boost stage, R_{T1} and R_{D1} are the on-resistance of the switch and diode of the buck stage, and R_{T2} and R_{D2} are the on-resistance of the switch and diode of the boost stage. The voltage sources U_{e1} and U_{e2} denote the equivalent voltage drops of the diodes in the buck stage and boost stage. These voltage sources do not influence the small signal model but alter the DC operating point of the system.

The inductor current, i_L, step responses for a small change (8%) in the buck-stage duty cycle, d_1, are shown in **Fig. 11**. The results from two typical operating points, a buck-boost mode (middle traces) and buck mode (bottom traces), are measured experimentally and compared with the theoretical responses. The figure shows that the theoretical model closely predicts the actual response. It can also be seen that the buck-boost mode of operation has higher damping and a longer time constant compared to the buck mode of operation.

B   Feed Forward Control and Current Loop Design

From the system small signal model, the transfer function $G_{d1i}(s)$ from buck stage duty cycle, d_1, to the inductor current, i_L, and the transfer function $G_{ui}(s)$ from the output voltage of boost stage, u_{C+}, to the inductor current, i_L, can be derived. Since the boost stages utilize hysteresis control, the output voltage u_{C+} can be assumed to be

Fig. 11   Comparison of the step responses between measurement results and calculation results, at the operating points of $D_1 = 0.5$ and $D_2 = 0.5$ (buck-boost mode) and $D_1 = 0.5$ and $D_2 = 0$ (buck mode). The operating parameters are: input voltage $U_{in} = 100$V, $R_L = 26\Omega$, $f_s = 100$kHz and component values given in the Appendix.
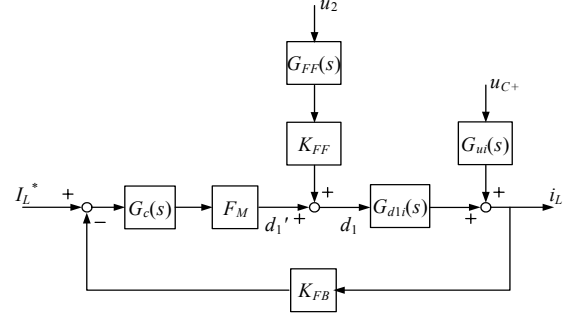

Fig. 12   Block diagram for inductor current control.

identical to the reference voltage (ignoring the switching noise and any small time delays). The output voltage of boost stage, u_{C+}, can be considered as a disturbance to i_L and therefore the focus is on analyzing $G_{d1i}(s)$ in order to design the proper controller $G_c(s)$ for the constant current control. The control block diagram for inductor current control schematic of Fig. 1(a) is illustrated in **Fig. 12**, where the inductor current feedback coefficient K_{FB} is 0.2; $G_{FF}(s)$ is the low pass filter for the feed forward voltage u_2, the feed forward coefficient $K_{FF} = 1/U_{in}$, and the triangular carrier coefficient F_M is the reciprocal value of the peak-to-peak amplitude of the triangular carrier.

The transfer function $G_{d1i}(s)$ can be derived as

$$G_{d1i}(s) = \frac{U_{in}}{s \cdot L + R_{total} - \frac{U_{C+} \cdot (1-D_2)}{I_L}} \tag{11}$$

where $R_{total} = R_{s,i1} + R_{e1} + R_{LM} + R_{e2} + R_{s,i2}$. For most operating points, the transfer function $G_{d1i}(s)$ has a pole in the right half plane, but by using feed-forward control the poles can be shifted to left half plane. The feed-forward effectively cancels the disturbance of u_{C+} and the transfer function $G_{d1'i}(s)$ can be derived as

$$G_{d1'i}(s) = \frac{U_{in}}{s \cdot L + R_{total}} \tag{12}$$

A PI controller with an additional pole at high frequency $G_c(s)$ is employed to compensate the system at the operating of $u_o = V_{op} \cdot \sin(0)$ to guarantee the system has a good performance at all operating points. The transfer function of $G_c(s)$ is given as
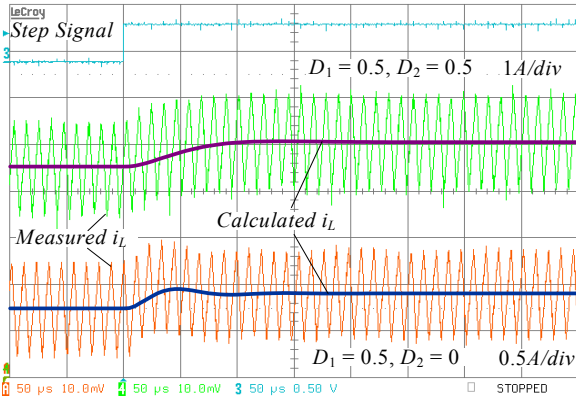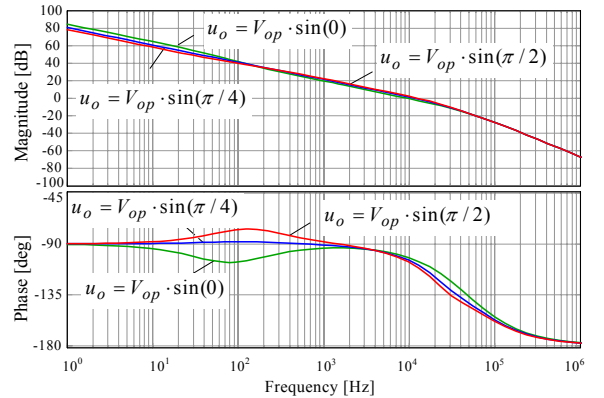

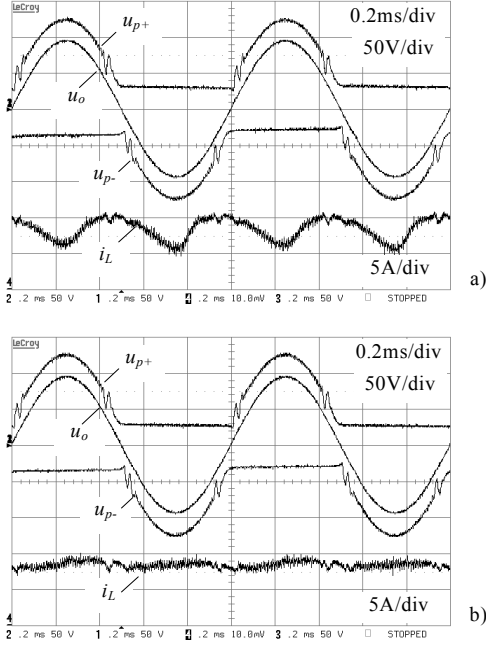**Fig. 13**   Bode plots of compensated system at three typical operating points.

Fig. 14 Performance comparison without feed-forward control (a) and with feed-forward control (b). Operating parameters are: $U_{in} = 100$ V, $I_L = 8$ A, $V_b = 30$ V, $V_{op} = 100$ V, $f_o = 1$ kHz, $R_L = 26$ Ω.

$$G_c(s) = K_P \frac{1 + s \cdot a_1}{s \cdot (1 + s \cdot b_1)} \qquad (13)$$

where $K_P = 50$, $a_1 = 4 \times 10^{-3}$ s^{-1}, $b_1 = 1.6 \times 10^{-6}$ s^{-1}.

With the designed controller, the inductor current loop has a phase margin of around 70° and an overall bandwidth of 10kHz, which is 10% of the switching frequency, as shown in **Fig. 13**.

The experimental results, measured from the laboratory prototype, are shown in **Fig. 14** and compared to the system performance without feed-forward control and with feed-forward control. It is shown that with the help of feed-forward control the shape of the inductor current I_L (Fig. 14 b)) shows a significant improvement in the rejection of the variation of output voltage compared to the inductor current I_L without feed-forward control (Fig. 14 a)).

V   ACTIVE DAMPING FOR OUTPUT FILTER

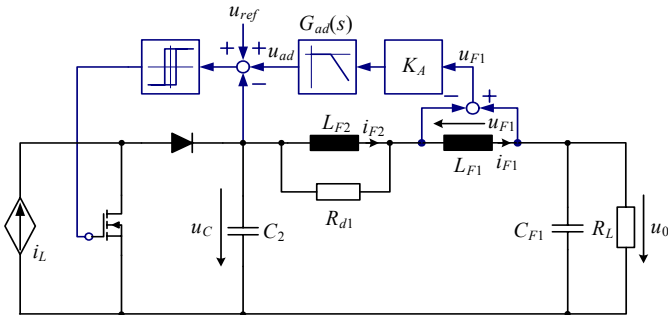In Fig. 14 it is also seen that the output voltages of the tracking

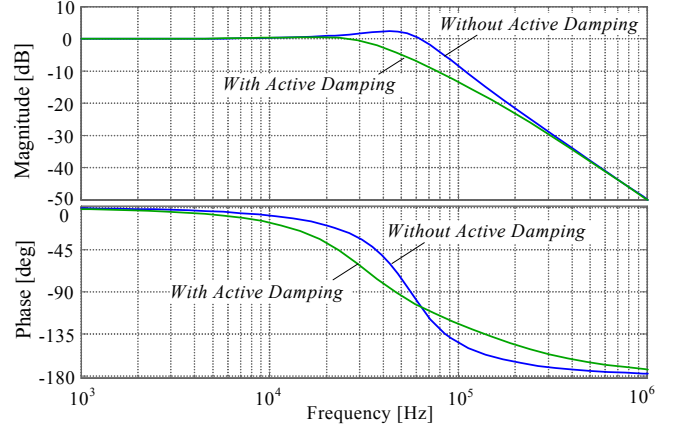**Fig. 15**   Structure for implementing active damping of the output filter.

Fig. 16   Comparison of the bode plots of the transfer function from u_{ref} to u_o with active damping and without active damping ($R_L = 26$Ω).

power supply have obvious oscillations when either upper transistors or lower transistors of the linear power amplifier start or stop conducting. One possible solution is to increase the passive damping of the output filter, but this would inevitably increase the system losses. The other possibility is to employ active damping of the output filter [11]. The structure used to implement the active damping is shown in **Fig. 15**. Since the capacitor voltage u_C is controlled by hysteresis controller, there is no direct access to control the duty cycle of the switch, and therefore the active damping signal alters the reference signal of the hysteresis controller. Active damping is implemented by measuring and low-pass filtering the filter inductor voltage u_{F1}, before adding it to the reference signal.

For the design the active damping the key point is to select a correct low-pass filter in order that the voltage u_{ad} at the natural frequency of the output filter has opposite phase as compared to u_{ref} to achieve a proper damping behavior. This filter should also be able to have sufficient attenuation of the switching frequencies. The value of the factor K_a should be selected carefully as increasing K_a can produce more damping, but also rise the risk of instability to the whole system.

A first-order low-pass filter with a corner frequency of 40kHz is selected as $G_{ad}(s)$, and K_a is selected as 2 V/V. **Fig. 16** compares the transfer function from u_{ref} to u_o (when R_L is 26Ω) with the case of active damping and without active damping. This figure shows that the damping of the system at the frequencies around the natural frequency of the output filter is significantly increased.

Experimental results are shown in **Fig. 17** to compare the system performance without active damping (a) and with active damping (b). It is shown that, the oscillations occurring in Fig. 17(a) disappeared in Fig. 17 (b) because of the active damping, but the switching noise is slightly increased as a result of the ripple components of u_{ad}, which should not be given in depth here due to the sake of brevity.

VI   CONCLUSIONS

This paper has presented a hybrid amplifier that is constructed from a linear power amplifier and a novel boost-type tracking power supply. The tracking power supply combines a buck and boost converter, with the boost converter operating with hysteresis control to provide a fast response. A procedure for the design of the output filter to limit the switching noise has been proposed using the PSRR of a linear power

Fig. 17 Comparison of the measured performance of the output voltages of the tracking power supply without active damping a) and with active damping b). The operation parameters are: $U_{in} = 100V$, $I_L = 8A$, $V_b = 30V$, $V_{op} = 100V$, $f_o = 1$ kHz, and $R_L = 26\Omega$.

amplifier. This method ensures that the amplifier output voltage has minimal switching frequency components but is also able to quickly track changes in the output voltage. A control system design method, using a small signal model of the linear amplifier, is used to ensure a good performance in the control of the constant inductor current and to provide a high rejection of any output voltage disturbances. The controller includes voltage feed forward to ensure stability over a wide range of operating points. Furthermore, an active damping method to reduce the oscillations in the output voltage produced by the output filter is implemented. A laboratory prototype experimentally verifies the theoretical analysis of the hybrid amplifier and shows that the combined system has an excellent performance.

ACKNOWLEDGMENT

APPENDIX

Table I lists the components used in the experimental hardware.

TABLE I: LIST OF POWER COMPONENTS OF THE TRACKING POWER SUPPLY

Name	Denomination	Type
Electrolytic Capacitor	C_{in}	$2 \times 470\mu F/220$ VDC
CoolMOS	T_1	SPW20N60C3
Power Diode	D_1	RHRG3060
Inductor	L_{M1}, L_{M2}	125µH, ELP 43/10/28
CoolMOS	T_2, T_3	SPW47N60C3
Power Diode	D_2, D_3	ISL9R1560P2
Film Capacitor	C_2, C_3	0.47µF/275 VAC
Output Filter inductor	L_{F1}, L_{F3}	24µH, 58550-A2
Damping inductor	L_{F2}, L_{F4}	34µH, 58550-A2
Output Filter Capacitor	C_{F1}, C_{F2}	0.33µF/275 VAC

REFERENCES

[1] Kashiwagi, S., "A High-Efficiency Audio Power Amplifier Using a Self-Oscillating Switching Regulator," *IEEE Trans. Industry Applications,* Vol.4, pp. 906-911, 1985.

[2] Soto, A., Oliver, J.A., Cobos, J.A., Cezon, J. and Arevalo, F., "Power Supply for a Radio Transmitter with Modulated Supply Voltage", in *Proc. 2004 Applied Power Electronics Conf.*, Vol. 1, pp. 392 – 398.

[3] Mikkel C. W. Hoyerby, Dnnis R. Andersen and Michael A. E. Andersen, "Tracking Power Supply for Automotive Multi-Channel-Single-Ended PWM Audio Amplifier System," in *Proc. 2004 International Power Electronics and Motion Control Conf.,* Riga, Latvia, Sept. 2 - 4, CD-ROM.

[4] Gong, G., Ertl, H., and Kolar, J.W., *"*High-Frequency Isolated DC/DC Converter for Input Voltage Conditioning of a Linear Power Amplifier," in *Proc. 2003 IEEE Power Electronics Specialists Conf.*, vol. 4, pp. 1929-34.

[5] Kolar, J.W., and Gong, G, "Vorrichtung zur Potentialtrennung und ausgangssignalabhängigen Führung der Versorgungsspannungen eines Linear-Leistungsverstärkers," *Swiss Patent Application*, filed April 2003.

[6] Douglas Self MA, "Audio Power Amplifier Design Handbook," 3rd ed., Newnes*,* 2002, pp. 247 – 253.

[7] Ribner, D.B., and Copeland, M.A., "Design Techniques for Cascoded CMOS Op Amps with Improved PSRR and Common-Mode Input Range," *IEEE Journal Solid-State Circuits*, Vol., 19, Issue, 6, pp. 919 – 925, 1984.

[8] Robert W. Erickson, "Fundamentals of Power Electronics," 2nd ed., Kluwer Academic Publishers, 2001, pp. 377 – 398.

[9] Heldwein, M.L., Nussbaumer, T., and Kolar, J.W., "Differential Mode EMC Input Filter Design for Three-Phase AC-DC-AC Sparse Matrix PWM Converters," in *Proc. 2004 IEEE Power Electronics Specialists Conf.*, Aachen, Germany, June 20 - 25, CD-ROM.

[10] Nussbaumer, T., Gong, G., Heldwein, M. L. and Kolar J. W., "Control-Oriented Modeling and Robust Control of a Three-Phase Buck+Boost PWM Rectifier," , to be published at *2005 IEEE Industrial Application Society Annual Meeting.*

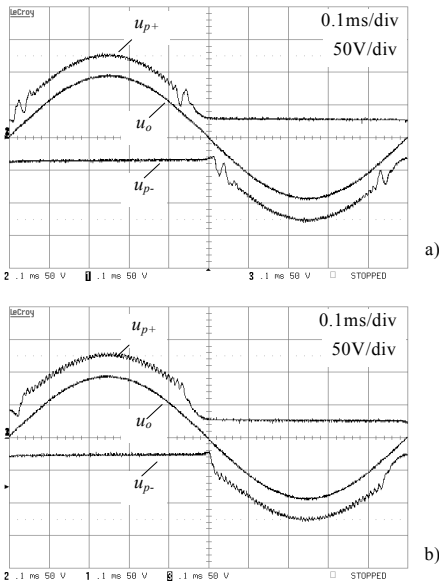[11] Sato, Y. and Kataoka, T., "A Current-Type PWM Rectifier with Active Damping Function," *IEEE Trans. on Industry Applications*, vol. 32, pp. 533 – 541, 1996.